Effect of light soaking on the electro- and photoluminescence of Cu(In,Ga)Se2 solar cells

T. C. M. Müller, T. M. H. Tran, B. E. Pieters, A. Gerber, R. Carius, and U. Rau

Citation: Applied Physics Letters **103**, 183504 (2013); doi: 10.1063/1.4827260
View online: http://dx.doi.org/10.1063/1.4827260
View Table of Contents: http://scitation.aip.org/content/aip/journal/apl/103/18?ver=pdfcov
Published by the AIP Publishing

Effect of light soaking on the electro- and photoluminescence of Cu(In,Ga)Se_2 solar cells

T. C. M. Müller, T. M. H. Tran, B. E. Pieters, A. Gerber, R. Carius, and U. Rau[a)]
IEK5-Photovoltaik, Forschungszentrum Jülich, 52425 Jülich, Germany

(Received 27 May 2013; accepted 14 October 2013; published online 30 October 2013)

ZnO/CdS/Cu(In,Ga)Se_2 solar cells are investigated by spectrally resolved electroluminescence and electro-modulated photoluminescence. The results agree well with the reciprocity relation between luminescence emission and photovoltaic quantum efficiency. In contrast, the superposition of photoluminescence and electroluminescence emission is warranted only in a limited injection range. At higher injection levels, we observe a characteristic discrepancy between electroluminescence and electro-modulated photoluminescence which is reduced by light soaking. We attribute this anomaly to a potential barrier close to the CdS/Cu(In,Ga)Se_2 interface. Hole injection into the space charge region during light soaking reduces this barrier and enhances the luminescence efficiency by a factor of 2.5. © *2013 AIP Publishing LLC*.
[http://dx.doi.org/10.1063/1.4827260]

Electroluminescence (EL) is the complementary physical action to the normal operating mode of a solar cell or module. Therefore, EL imaging[1] is an attractive tool for the characterization of such devices, e.g., for the analysis of resistive and recombination losses.[2,3] As a direct semiconductor, Cu(In,Ga)Se_2 (CIGS) is especially suitable for luminescence based methods and EL was frequently used for the spectral,[4,5] or spatial[6–9] analysis of CIGS cells and modules in the past. However, CIGS solar cells and modules are subject to metastable changes of their electronic properties upon voltage and/or light bias.[10–13] These metastable changes are an intrinsic property of the CIGS absorber material and are due to the (V_{Cu}, V_{Se}) divacancy complex[14] and the In_{Cu} antisite defect.[15] Since both defects exist in multiple charge states, their influence on the electronic behavior of CIGS solar cells is rather complex. Already in equilibrium the divacancy complex has three different charge configurations, namely, $(V_{Cu},V_{Se})^{+}$, $(V_{Cu},V_{Se})^{-}$, and $(V_{Cu},V_{Se})^{3-}$, dependent on the position in the band diagram of the ZnO/CdS/CIGS heterostructure.[14,16,17] It was recently shown that metastabilities are detectable in EL images of CIGS solar modules and considerably influence their quantitative interpretation.[18]

The present letter investigates the consequences of light soaking (LS) on the fundamental properties of electro- and photoluminescence (PL) properties of CIGS solar cells. We especially address the question whether the reciprocity relation[19,20] between electroluminescence emission, photoluminescence emission and external photovoltaic quantum efficiency $Q_e(E)$ apply to these solar cells.

The reciprocity relation reads

$$\begin{aligned}\phi_{em}(E) &= \phi_{SC}(E,\phi_{exc}) + \phi_{EL}(E,V_j)\\ &= \phi_{SC}(E,\phi_{exc}) + Q_e(E)\phi_{bb}(E)\left[\exp\left(\frac{qV_j}{kT}\right) - 1\right],\end{aligned} \tag{1}$$

where $\phi_{bb}(E)$ denotes the spectral photon flux density of a black body, V_j the voltage applied to the junction, and kT/q the thermal voltage. In Eq. (1), the emitted photon flux density $\phi_{em}(E)$, as a function of photon energy E, is a superposition of the pure EL emission ϕ_{EL} stimulated by the junction voltage V_j and the short circuit (SC) emission ϕ_{SC} caused by the photoexcitation ϕ_{exc}. Equation (1) describes (i) a quantitative relation between ϕ_{em} and $Q_e(E)$ and also states (ii) a linear superposition of the voltage driven (EL) and SC emission, (iii) that the spectral shape of this emission is unaltered at different bias conditions, and (iv) that the EL emission ϕ_{em} follows a diode law with an ideality factor of unity like in the detailed balance theory for solar cells of Shockley and Queisser.[21] This expected behavior is analogous to the usual diode ideality factor n_{id} which in most cases represents non-radiative recombination. This ideality factor is unity in Shockley's classical diode theory[22] and deviations from this value (usually $n_{id} > 1$) are indicative for a situation that is not described by the principle of detailed balance. Therefore, we define a radiative ideality factor n_{rad} according to

$$n_{rad} = \frac{q}{kT}\left\{\frac{d}{dV_j}\ln\left[\int\phi_{EL}(E)dE\right]\right\}^{-1}, \tag{2}$$

allowing us to determine experimentally whether or not the radiative behavior of a solar cell, or likewise a light emitting diode, deviates from the predictions of Eq. (1).

The validity of implications (i) to (iv) is especially important for spatially resolved EL measurements where in most cases the camera signal S_{cam} is interpreted using the proportionality[3,23]

$$S_{cam} \propto \exp\left(\frac{qV_j}{kT}\right), \tag{3}$$

i.e., neglecting the short circuit term in Eq. (1). However, because of the spectrally dependent quantum efficiency $Q_{cam}(E)$ of the camera, we also have

[a)]Author to whom correspondence should be addressed. Electronic mail: u.rau@fz-juelich.de

$$S_{\mathrm{cam}} = \int Q_{\mathrm{cam}}(E)\phi_{\mathrm{EL}}(E)dE. \quad (4)$$

Therefore, the validity of Eq. (1), with all four implications, is a precondition for the usage of Eq. (3). Up to present, experimental investigations concentrated on the verification of (i) and (iii) for the cases of Si wafer cells,[4,24] CIGS thin-film cells,[4,5] organic solar cells,[25] and GaInP/InGaAs/Ge multijunction solar cells.[26,27]

At this point, it is important to note that the reciprocity relation is derived from the principle of detailed balance, more precisely, from an extrapolation of all equilibrium rate constants towards a non-equilibrium situation. Thus, Eq. (1) connects the result of a small-signal analysis, namely, the quantum efficiency, derived relatively close to thermal equilibrium, with the electroluminescent emission of the same device, measured considerably far from equilibrium. Moreover, the collecting/injecting junction enters in the derivation[19,20] of Eq. (1) as a mere boundary condition. This is the reason why, for pin type solar cells, Eq. (1) is only strictly valid in the limit of high charge carrier mobilities: The quasi-Fermi levels through the space charge region (SCR) must be flat under any bias voltage, and the charge carrier collection efficiency within the SCR must be unity.[28] In addition, non-linear occupation terms dominating radiative recombination via tail states are not necessarily compatible with reciprocity.[29,30]

In a typical CIGS solar cell, the SCR is about one third of the absorber thickness[31] putting the electrostatic properties of the device somewhere in between a pure pin-type solar cell and a pn-type cell with a negligible width of the SCR like in wafer based crystalline silicon solar cells. It is also known that tail-like states play a role in non-radiative recombination of these devices.[32,33] For all these reasons, a careful investigation of the validity of Eq. (1) for CIGS based solar cells is necessary to ensure an appropriate evaluation of luminescence measurements of these devices on the basis of reciprocity.

The solar cell under investigation ($4.5 \times 9.7\,\mathrm{mm}^2$) was cut from a CIGS modules produced industrially (efficiency $\eta = 12.7\%$, open circuit voltage $V_{\mathrm{OC}} = 665\,\mathrm{mV/cell}$) by an in-line co-evaporation process on a Mo-covered glass substrate finished by a chemical bath deposition of the CdS layer and by sputtering of the transparent ZnO window layer.[34] EL and PL spectra were recorded using a Fourier Transform Infrared Spectrometer (FTIR) equipped with a liquid nitrogen cooled germanium detector. The spectral response of the system was calibrated by a tungsten calibration lamp. EL measurements were performed by applying a periodic rectangular AC voltage between $V_{\mathrm{j}} = 0\,\mathrm{V}$ and a forward bias voltage (V_{j}) for charge carrier injection. Signal detection was carried out using a lock-in amplifier in conjunction with the step-scan mode of the spectrometer. For the PL measurement, we used a widened laser illumination (combined solid state laser with wavelengths of 473, 532, and 671 nm) and an electro-modulation technique (EM) switching the applied junction voltage between $V_{\mathrm{j}} = 0\,\mathrm{V}$, i.e., SC, and $V_{\mathrm{j}} = V_{\mathrm{oc}}$, i.e., to the open circuit voltage of the corresponding illumination level.[35] We expect from Eq. (1) that the modulation technique yields quantitatively the same emission as the EL technique, i.e., $\phi_{\mathrm{EM}}(E) = \phi_{\mathrm{EL}}(E)$. Before the measurement of the device in the initial state (before LS), the device was stored in the cryostate at room temperature for more than 10 h. After the first analysis, LS was performed at an elevated temperature $T_{\mathrm{LS}} = 400\,\mathrm{K}$ for 5 h with illumination intensity of approximately 1 sun. During that time the open circuit voltage (V_{oc} at 400 K) increased by 28 mV, reaching saturation after 3 h. The analysis of the light soaked state took place at 300 K immediately after the LS. At 300 K the V_{oc} difference between initial and light soaked state amounted to $\Delta V_{\mathrm{oc}} = 28\,\mathrm{mV}$. During the entire analysis cycle the sample was kept in the cryostate.

Figure 1 shows the measured external quantum efficiency $Q_{\mathrm{e}}(E)$ together with the EL emission $\phi_{\mathrm{EL}}(E)$ of the same device. The data for $Q_{\mathrm{e}}(E)$ and $\phi_{\mathrm{EL}}(E)$ recalculated from the respective other measurement with the help of Eq. (1) are also shown. The predictive power of Eq. (1) is well demonstrated in the relevant overlap region of photon energies $1.15\,\mathrm{eV} \le E \le 1.30\,\mathrm{eV}$, especially by the fact that the $Q_{\mathrm{e}}(E)$ spectrum accurately predicts the maximum of the EL emission. Thus, the reciprocity between Q_{e} and ϕ_{EL} [implication (i)] is valid not only for high-efficiency CIGS cells from the laboratory,[4,5] but also for these cells made from industrially produced modules.

Next, we test prediction (ii) and (iii), namely, the fact that the spectral shape of the EL emission is unaltered under different bias conditions and corresponds to the spectra obtained by the EM method. Figure 2 compares EM and EL measurements obtained at the same injection level which was achieved by the following method: During the EM measurements the short circuit current density J_{SC} induced by the laser illumination was recorded. Subsequently, the current density J injected during the following EL measurement was adjusted to the previous JSC from the EM measurement within an accuracy of 4%. Figure 2(a) shows spectra before and Fig. 2(b) after LS. The spectral shape of all emissions neither does change by changing the applied bias nor between EL an EM measurements. Additionally, the spectral shape is not affected by LS.

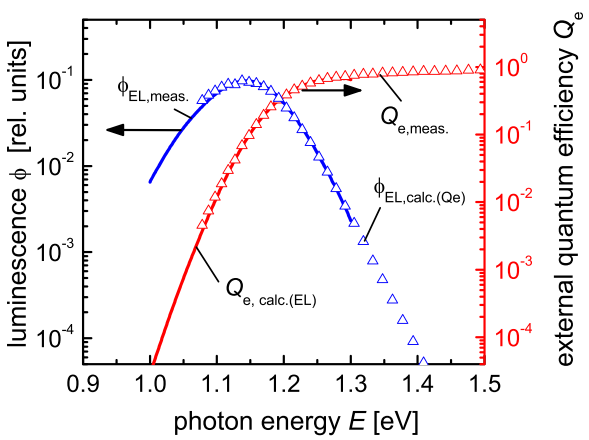

FIG. 1. Measured EL spectrum $\phi_{\mathrm{EL,meas.}}(E)$ obtained from a CIGS solar cell and the external quantum efficiency $Q_{\mathrm{e,\,calc.(EL)}}(E)$ calculated from $\phi_{\mathrm{EL,meas.}}(E)$with the help of Eq. (1) (solid line). Open triangles show the directly measured $Q_{\mathrm{e,meas.}}(E)$ and the EL spectrum $\phi_{\mathrm{EL,\,calc.(Qe)}}(E)$calculated from the experimental$Q_{\mathrm{e,meas.}}(E)$.

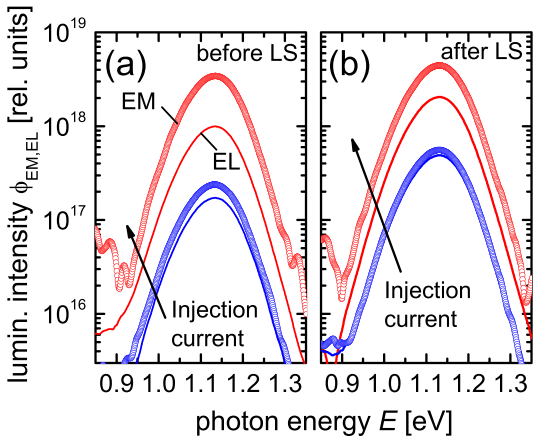

FIG. 2. Electroluminescence (solid lines) and electro-modulated photoluminescence (open circles) spectra from a CIGS solar cell under different current injection conditions at temperature $T = 300$ K. (a) Spectra taken before light soaking ($J = 35.85$, 7.31 mA/cm^2), (b) spectra after light soaking for 3 h at an elevated temperature, $T_{LS} = 400$ K ($J = 26.01$, 6.82 mA/cm^2).

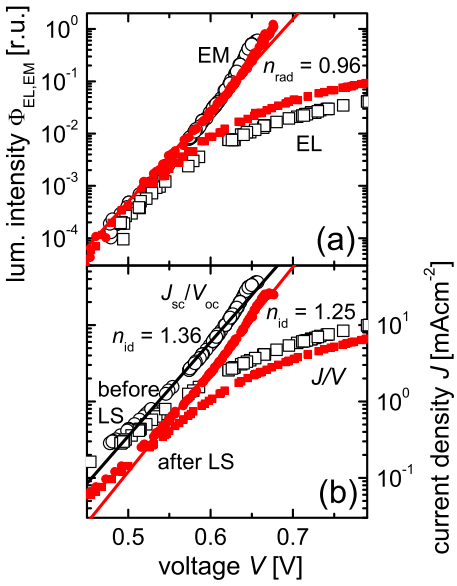

FIG. 3. (a) Voltage dependence of the omni-spectral EL $\Phi_{EL}(V)$ before/after LS (open/full squares), and dependence of the EM signal $\Phi_{EM}(Voc)$ on the open circuit voltage V_{OC} (open filled circles) obtained from the same CIGS solar cell as in Figs. 2 and 3. The *radiative* ideality factor $n_{rad} = 0.96$ results from the fit (red solid line) to $\Phi_{EM}(Voc)$ after and before LS. (b) Short circuit current density vs. open circuit voltage (J_{SC}/V_{OC}) measured simultaneously to the EM measurements and current density vs. voltage (J/V) measurement carried out simultaneously to the EL measurements before (open symbols) and after LS (full symbols). The (non-radiative) ideality $n_{id} = 1.36$ and 1.25 (before/after LS) is obtained from the J_{SC}/V_{OC} characteristics and corresponds to the classical diode ideality factor.

It is however evident that the intensity of the EM emission is higher than that of the EL emission taken at a current density equaling the short circuit current density of the EM measurement. To investigate this unexpected effect closer, we have measured the omni-spectral EL and EM for a larger series of injection densities using the Ge detector without FTIR. Because the spectral shape of the emission is unaltered under different bias conditions the detector signal $S_{det}(V)$, given by Eq. (4) is proportional to the omnispectral luminescence signal $\Phi = \int \phi(E)dE$ at any the external voltage or, likewise at any incident irradiation intensity, regardless of the quantum efficiency Q_{det} of the detector.

Figure 3(a) shows the integral EL and EM intensities before and after LS respective to the applied voltage V_j (EL) or the measured open circuit voltage V_{OC} (EM). Due to the series resistance, the EL data saturate towards higher voltages, whereas the EM data approximately represent straight lines. A fit to the EM data before and after LS yields a *radiative* ideality factor $n_{rad} \approx 0.96$, which is fairly close to unity. The small reduction of n_{rad} below unity could result from a (slight) voltage bias dependence of current collection.[36] However, more important is the finding that for voltages above 0.6 V both curves (before and after LS) increasingly deviate from the straight line obtained at low injection.

Figure 3(b) displays the classical dark current/voltage (J/V) characteristics for both states, where the data are taken simultaneously to the EL measurements. In addition, Fig. 3(b) shows the short circuit current density vs. open circuit voltage (J_{SC}/V_{OC}) characteristics measured simultaneously to the EM spectra as their characteristic values. The dark J/V characteristics are entirely dominated by the series resistance. The J_{SC}/V_{OC} curves do not follow a perfect diode law, possibly also due to a bias dependence of carrier collection.[36] However, fitting a straight line to the curves characteristics allow for an approximate determination of the classical (non-radiative) ideality factor as $n_{id} \approx 1.36$ and 1.25 (before and after LS, respectively). These values are markedly different from the radiative ideality factor n_{rad} determined from Fig. 3(a).

Figure 4(a) plots the luminescence intensities vs. the measured current densities, eliminating in this way the voltage as a parameter and also the influence of the series resistance. We see that the data in a large part of the double logarithmic plot fall on a straight line with a slope Γ that corresponds to the ratio of non-radiative and radiative ideality factor according to

$$\Gamma = \frac{d\Phi_{EM}}{dV_{OC}}\frac{1}{\Phi_{EM}} \Big/ \left(\frac{dJ}{dV}\frac{1}{J}\right) = \frac{n_{id}}{n_{rad}}. \quad (5)$$

However, for current densities $J > 4\,\mathrm{mA\,cm^{-2}}$ and $J > 15\,\mathrm{mA\,cm^{-2}}$ (before and after LS), the experimental data significantly deviate from the straight line and EL/EM data deviate from each other. This significant anomaly is partly healed by LS such that after the procedure, the device is well behaved in a significant range nearly up to the one sun equivalent of short circuit current density. Figure 4(b) depicts the external luminescence efficiencies Q_{LED} and Q_{lum}, i.e., the ratios between radiative and non-radiative recombination[19] that are obtained via

$$Q_{LED/lum} \propto \Phi_{EL/EM}/J. \quad (6)$$

In Fig. 4(b), it becomes clear that LS improves the luminescence efficiencies by about a factor of 2.5. This finding fits to classical explanation that the effect of persistent conductivity reduces the space charge region and herewith the amount of non-radiative recombination. Quantitatively, the LS induced increase $\Delta V_{oc} = 28$ mV fits $\approx n_{id}kT/q \times \ln(2.5)$ reflected the shift of the J_{SC}/V_{OC} and the J/V characteristics towards higher voltages in Fig. 3(b). At the same time, the $\Phi_{EM}(V_{OC})$ and the $\Phi_{EL}(V_j)$ characteristics in Fig. 3(a) are

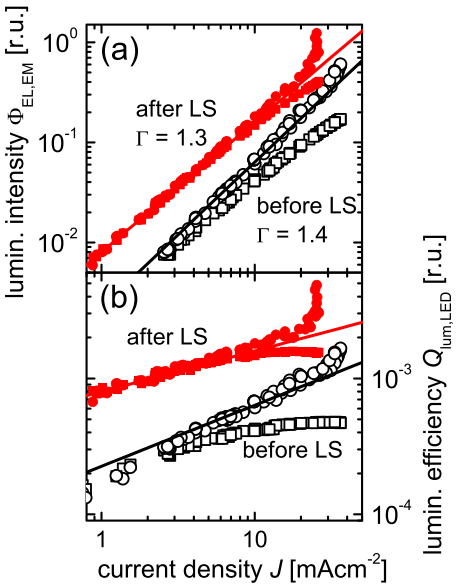

FIG. 4. (a) Dependence of the omni-spectral EL Φ_{EL} before/after light soaking (LS) (open/full squares) on the current density J, and dependence of the EM signal Φ_{EM} (open/full circles) on the short circuit current density J_{SC}. The slopes Γ of the curves follow from the ratio between non-radiative and radiative ideality factors from Fig. 4 according to Eq. (5). (b) External luminescence quantum efficiencies Q_{LED} calculated from Φ_{EL} and Q_{lum} and calculated from Φ_{EM} with the help of Eq. (6). The straight lines are directly calculated from the two slopes Γ in (a) and correspond to Γ-1 in (b), respectively.

much less affected by LS, except for a reduction in series resistance seen in $\Phi_{EL}(V_j)$.

The mentioned anomaly is also clearly seen in Fig. 4(b) where the EL efficiency Q_{LED} appears to saturate at current densities $J > 10\,\mathrm{mA\,cm^{-2}}$. Simultaneously, the EM luminescence efficiency (Q_{lum}) increases. In other words, photo-generated charge carrier injection by illumination is increasingly decoupled from charge carrier collection and non-radiative recombination. This behavior is clearly in conflict with the superposition principle as expressed by Eq. (1).

The difference of radiative and non-radiative ideality factors tells us that radiative and non-radiative recombination paths are different. Radiative recombination in CIGS at room temperature is a band-to-band like mechanism involving relatively steep band-tails or relatively small spatial band edge fluctuations.[5] This fact is proven by the invariance of the emission spectra under different bias conditions. The close-to-unity *radiative* ideality factor n_{rad} also points into that direction. It is safe to assume that the luminescence emission monitors the entire bulk of the CIGS. In contrast, the larger ideality factor n_{id} of the dominating non-radiative recombination path points to the space charge region as the dominant location of recombination[32] involving also deeper states or tail states with large Urbach energy. The difference of the two ideality factors is responsible for the fact that the luminescence efficiencies gradually increase with increasing electrical or light bias.

Up to this point, the observations are not surprising: Radiative and non-radiative recombination using different electronic states situated at different energies and locations is a common feature of semiconductor materials. More surprising is the divergence of EL and EM under high bias conditions (Figs. 4(a) and 4(b)). A possible explanation for these observations is that under high light injection (EM above 0.65 V), the splitting of the quasi-Fermi levels in the bulk of the material (as the origin of the luminescence) is larger than the open circuit voltage V_{OC} detected at the terminals of the device. Such a situation could be realized by an electrostatic barrier between the main part of the CIGS bulk and the main region of non-radiative recombination.[37] In turn for the EL situation, the same barrier would hinder injection of electrons from the junction into the bulk, thereby limiting the EL emission from the bulk up to the observed saturation of Q_{LED}. The metastable (V_{Cu},V_{Se}) divacancy complex with three different charge states[14] possibly could provide an explanation for our observations. However, more quantitative insight should come from numerical device simulations.

In summary, spectrally resolved measurements of EL and of electro-modulated PL unveil a distinct picture of the metastable behavior of CIGS based devices. The observed divergence of EL and EM under high bias conditions and its dependence on the LS history could be a key for the understanding of metastable defects in CIGS and their consequences for the device performance. Thus, luminescence analysis turns out as a powerful tool to analyze the metastable device behavior of CIGS in detail. Metastabilities in CIGS decisively depend on the details of absorber and interface preparation, and the presented luminescence methods provide a sensitive way to compare the specific differences.

The present work has been supported by the German Ministry of Environment under Contract No. FKZ 0325149. The authors thank R. Schäffler and J. P. Theisen (Würth Solar) for providing the CIGS modules, T. Kirchartz (Imperial College), R. Scheer (Universität Halle), and J. R. Sites (Colorado State University) for helpful discussions.

[1]T. Fuyuki, H. Kondo, T. Yamazaki, Y. Takahashi, and Y. Uraoka, Appl. Phys. Lett. **86**, 262108 (2005).
[2]T. Trupke, R. A. Bardos, M. C. Schubert, and W. Warta, Appl. Phys. Lett. **89**, 044107 (2006).
[3]K. Ramspeck, K. Bothe, D. Hinken, B. Fischer, J. Schmidt, and R. Brendel, Appl. Phys. Lett. **90**, 153502 (2007).
[4]T. Kirchartz, U. Rau, M. Kurth, J. Mattheis, and J. H. Werner, Thin Solid Films **515**, 6238 (2007).
[5]T. Kirchartz and U. Rau, J. Appl. Phys. **102**, 104510 (2007).
[6]A. Helbig, T. Kirchartz, R. Schaeffler, J. H. Werner, and U. Rau, Sol. Energy Mater. Sol. Cells **94**, 979 (2010).
[7]G. Brown, A. Pudov, B. Cardozo, V. Faifer, E. Bykov, and M. Contreras, J. Appl. Phys. **108**, 074516 (2010).
[8]S. Johnston, T. Unold, I. Repins, R. Sundaramoorthy, K. M. Jones, B. To, N. Call, and R. Ahrenkiel, J. Vac. Sci. Technol. A **28**, 665 (2010).
[9]M. Paire, L. Lombez, J.-F. Guillemoles, and D. Lincot, Thin Solid Films **519**, 7493 (2011).
[10]M. Igalson and H. W. Schock, J. Appl. Phys. **80**, 5765 (1996).
[11]U. Rau, M. Schmitt, J. Parisi, W. Riedl, and F. Karg, Appl. Phys. Lett. **73**, 223 (1998).
[12]P. Zabierowski, U. Rau, and M. Igalson, Thin Solid Films **387**, 147 (2001).
[13]J. T. Heath, J. D. Cohen, and W. N. Shafarman, J. Appl. Phys. **95**, 1000 (2004).
[14]S. Lany and A. Zunger, J. Appl. Phys. **100**, 113725 (2006).
[15]S. Lany and A. Zunger, Phys. Rev. Lett. **100**, 016401 (2008).
[16]R. Urbaniak and M. Igalson, J. Appl. Phys. **106**, 063720 (2009).
[17]S. Siebentritt, M. Igalson, C. Person, and S. Lany, Prog. Photovoltaics **18**, 390 (2010).

[18]T. M. H. Tran, B. E. Pieters, C. Ulbrich, A. Gerber, T. Kirchartz, and U. Rau, Thin Solid Films **535**, 307 (2013).
[19]U. Rau, Phys. Rev. B **76**, 085303 (2007).
[20]U. Rau, IEEE J. Photovoltaics **2**, 169 (2012).
[21]W. Shockley and H. J. Queisser, J. Appl. Phys. **32**, 510 (1961).
[22]W. Shockley, Bell Syst. Tech. J. **28**, 435 (1949).
[23]P. Würfel, T. Trupke, T. Puzzer, E. Schäffer, W. Warta, and S. W. Glunz, J. Appl. Phys. **101**, 123110 (2007).
[24]T. Kirchartz, A. Helbig, W. Reetz, M. Reuter, J. H. Werner, and U. Rau, Prog. Photovoltaics **17**, 394 (2009).
[25]K. Vandewal, K. Tvingstedt, A. Gadisa, O. Inganas, and J. V. Manca, Nature Mater. **8**, 904 (2009).
[26]T. Kirchartz, U. Rau, M. Hermle, A. W. Bett, A. Helbig, and J. H. Werner, Appl. Phys. Lett. **92**, 123502 (2008).
[27]S. Roensch, R. Hoheisel, F. Dimroth, and A. W. Bett, Appl. Phys. Lett. **98**, 251113 (2011).
[28]T. Kirchartz and U. Rau, Phys. Status Solidi A **205**, 2737 (2008).
[29]B. E. Pieters, T. Merdzhanova, T. Kirchartz, and R. Carius, Sol. Energy Mater. Sol. Cells **94**, 1851 (2010).
[30]T. C. M. Müller, B. E. Pieters, T. Kirchartz, R. Carius, and U. Rau, Phys. Status Solidi C **9**, 1963 (2012).
[31]U. Rau and H. W. Schock, Appl. Phys. A **69**, 131 (1999).
[32]T. Walter, R. Herberholz, and H. W. Schock, Solid State Phenom. **51–52**, 309 (1996).
[33]U. Rau, A. Jasenek, H. W. Schock, F. Engelhardt, and T. Meyer, Thin Solid Films **361–362**, 298 (2000).
[34]B. Dimmler, M. Powalla, and R. Schaeffler, in *Proceedings of the 31st IEEE Photovoltaic Specialists Conference* (IEEE, New York, 2005), p. 189–194.
[35]T. Merdzhanova, R. Carius, S. Klein, F. Finger, and D. Dimova-Malinovska, Thin Solid Films **451–452**, 285 (2004).
[36]M. Eron and A. Rothwarf, Appl. Phys. Lett. **44**, 131 (1984).
[37]R. Kniese, M. Powalla, and U. Rau, Thin Solid Films **515**, 6163 (2007).